AIAA JOURNAL
Vol. 44, No. 9, September 2006

Investigation of Nonreflective Boundary Conditions for Computational Aeroacoustics

Mirela Caraeni*
Fluent Inc., Lebanon, New Hampshire 03766
and
Laszlo Fuchs†
Lund Institute of Technology, 221 00 Lund, Sweden

DOI: 10.2514/1.5807

Direct aeroacoustic computations require nonreflective boundary conditions that allow disturbances to leave the domain freely without anomalous reflections. In the present paper we analyze a series of nonreflective boundary conditions already published in the literature and propose an improved outflow nonreflective boundary condition with reflection characteristic that is reduced greatly. For the solution of the linearized Euler equations, a sixth-order compact finite-difference algorithm is used together with a sixth-order explicit digital filter that suppresses the high-frequency spurious oscillations in the solution. A number of representative test cases are presented. The new outflow boundary condition is recommended for the simulation of sound produced by turbulence.

I. Introduction

SOLVING a problem formulated on an unbounded domain usually requires truncating the domain and solving the artificial boundary conditions (ABCs) at the newly external boundary. ABCs appear in many areas of scientific computing such as acoustics, electrodynamics, solid mechanics, and fluid dynamics (see reviews by Givoli [1], Tsynkov [2], and Hagstrom [3]).

The techniques used currently to set the ABCs can be classified into two groups. The methods from the first group, called global ABCs in Tsynkov [2], provide high accuracy and robustness of the numerical procedure, but seem to be cumbersome and computational expensive. The methods from the second group, called local ABCs, are algorithmically simple, numerically cheap, and geometrically universal, but usually lack accuracy.

We review the ABCs for simulation of inflow and outflow problems with an emphasis on techniques suitable for compressible turbulent flows.

Numerical simulations of sound propagation in the far field are based usually on the linearized Euler (LEE) or linearized Navier–Stokes (LNSE) equations together with appropriate boundary conditions (BC) for inflow and outflow problems. These boundary conditions should allow the flow disturbances, like the pressure (acoustic disturbances), vorticity, or entropy perturbations, etc., to leave the computational domain without significantly affecting them and most importantly without reflections. This is very important in computational aeroacoustics (CAA), because the spurious (acoustic) waves generated by inadequate boundary conditions can mask the true sound field, when the simulation is done far from the sources of sound. For this type of simulation, state-of-the-art nonreflective boundary conditions (NRBC) have been proposed by Giles [4], Colonius et al. [5], Tam [6], etc.

Following the above classification, today's state-of-the-art nonreflective boundary conditions can be grouped as the following:

1) Global ABCs, see, for instance, the boundary conditions developed by Thompson [7], Poinsot and Lele [8], Colonius et al. [5], Bogey and Bailly [9], etc. This group develops nonreflective boundary conditions based on characteristics theory. The main idea is to cast the linearized Euler equations into a reference frame relative to the boundary normal, in terms of the Riemann invariants. These Riemann invariants are the acoustic, entropy, and vortical invariants. The nonreflective boundary condition will simply impose the value (zero) of the incoming invariants. Work by Watson and Zorumski [10] is extended to treat the one-dimensional time-periodic duct acoustic phenomena described by the linearized Euler equations in the far field (the one-dimensional methodology of Watson [10] does admit a multidimensional generalization, see Colonius [5]).

2) Local ABCs, see boundary conditions suggested by Bayliss and Turkel [11], derive nonreflective boundary conditions based on the far-field asymptotics for the solution of the two-dimensional linearized Euler equations and construct the first-order local ABCs for the calculation of acoustic fields in uniformly moving media; see Tam and Webb [12]. Tam's two-dimensional boundary conditions have been extended for the case of nonuniform flow by Tam and Dong [13].

Colonius [14] discusses various models for an outflow boundary in the nonlinear case, such as absorbing layers and fringe methods. For an inflow and outflow boundary, Freund [15] provides a general framework for addressing the generalized buffer zone technique. For the case of a turbulent jet where the artificial boundary intersects the source region, he suggests the use of an additional buffer layer scheme. Thus, an additional layer of several grid points is added to the computational domain and the governing equations are modified or amended in this buffer layer so as to absorb or dissipate the waves and to prevent wave reflection back to the solution domain. For this kind of boundary treatment, we mention here the perfectly matched layer (PML) and the sponge-layer schemes.

The PML scheme has been introduced by Berenger [16,17]. In this scheme the governing equations are split according to the spatial derivatives. Furthermore, the dependent variables are also split into subcomponents and an absorption coefficient is introduced into these equations. The resulting PML equations are solved within the PML domain. The procedure originally developed by Berenger with applications to electromagnetic waves has been extended to linearized Euler equations by Hu [18], Tam [19] and Euler equations by Hu [20].

The sponge-layer scheme requires the introduction of an additional layer where a source term is added to the governing equation with the objective to dissipate the wave within the sponge layer. The source term to be added to the right-hand side (RHS) of the governing equation is $\sigma(x)\bar{Q}$, where

Received 14 October 2003; revision received 24 April 2006; accepted for publication 4 May 2006.

*Ph.D.; mlc@fluent.com.
†Professor, LTH; lf@mail.vok.lth.se.

$$\sigma(x) = \begin{cases} a[(x - x_B)/(x_B - x_E)]^n, & x_B \le x \le x_E \\ 0, & \text{otherwise} \end{cases} \quad (1)$$

This expression is used for the sponge layer at the boundary perpendicular to the x axis. A similar expression is written for the boundary perpendicular to the y axis. Terms x_B and x_E in relation (1) denote the x coordinates of the beginning and the end of the sponge layer, respectively. The constants a and n are specified to control the amplitude and distribution of the damping coefficient σ. The implementation of the sponge-layer concept is simple and straightforward without any major modification of the governing equations.

First, the numerical scheme used in this work is presented; more details can be found in Caraeni [21]. Then, we investigate a series of published nonreflective boundary conditions and propose an improved outflow boundary condition for computational aeroacoustics and the simulation of sound produced by turbulence. The newly proposed outflow boundary condition reduces significantly the appearance of spurious pressure disturbances, abnormally produced in the outflow by the exit of weak vortical structures (of turbulence, etc.) or by oblique sound waves. Test cases are presented to address the accuracy of the new boundary condition and also for the other boundary conditions investigated.

II. Linearized Euler Equations

Nonreflective boundary conditions are typically derived for linear hyperbolic systems. Let us consider the linearized Euler equations written in primitive variable formulation, in 2-D. Consider the following decomposition of the primitive variable vector:

$$\mathbf{q} = q_0 + q \quad (2)$$

where $\mathbf{q}$, q_0, and q are the instantaneous, mean (uniform), and perturbation values of the field vector $(\boldsymbol{\rho}, \mathbf{u}, \mathbf{v}, \mathbf{p})^T$. Here, $\mathbf{u}, \mathbf{v}$ are the instantaneous velocities in the x and y directions, $\boldsymbol{\rho}$ and $\mathbf{p}$ the (instantaneous) density and pressure, respectively. The linearized Euler equations can be written in nonconservative form as

$$\frac{\partial q}{\partial t} + \mathcal{A}\frac{\partial q}{\partial x} + \mathcal{B}\frac{\partial q}{\partial y} = \mathbf{S} \quad (3)$$

were $q = (\rho, u, v, p)^T$ is the perturbed primitive variable vector,

$$\mathcal{A} = \begin{bmatrix} u_0 & \rho_0 & 0 & 0 \\ 0 & u_0 & 0 & \frac{1}{\rho_0} \\ 0 & 0 & u_0 & 0 \\ 0 & \gamma p_0 & 0 & u_0 \end{bmatrix} \quad (4)$$

$$\mathcal{B} = \begin{bmatrix} v_0 & \rho & 0 & 0 \\ 0 & v_0 & 0 & 0 \\ 0 & 0 & v_0 & \frac{1}{\rho_0} \\ 0 & 0 & \gamma p_0 & v_0 \end{bmatrix} \quad (5)$$

are the convective-flux Jacobians, computed for $q_0 = (\rho_0, u_0, v_0, p_0)^T$. Note that the source term $\mathbf{S}$ can be a function of space and time $\mathbf{S} = \mathbf{S}(x, y, t)$. Here, the term $\mathbf{S}$ has been introduced in the linearized Euler equations for convenience. It is only used when prescribing (space and time dependent) sources of perturbation for sound, entropy, etc., in the computational domain; see, for example, Sec. VII.C.

Typically, the background conditions described by q_0 represent either uniform mean conditions or a solution of the steady linearized Euler equations. For far-field sound propagation we assume here uniform mean conditions, for example, $q_0 = \text{const}$.

III. Spatial Discretization

Compact-finite differences are renowned for their high accuracy and computational efficiency and have been traditionally employed in CAA. Here we use a compact finite-difference discretization scheme on a uniform, structured Cartesian mesh. Let us consider Eq. (3), written in semidiscrete form:

$$\frac{\partial q}{\partial t} = -\mathcal{A}_{(q_0)}\left(\frac{\partial q}{\partial x}\right)^{\text{num}} - \mathcal{B}_{(q_0)}\left(\frac{\partial q}{\partial y}\right)^{\text{num}} + \mathbf{S}^{\text{num}} \quad (6)$$

where the superscript "num" symbolizes the values of the corresponding derivatives and the source term computed numerically.

In the present work we employ a sixth-order, five-point stencil compact finite-difference formula to compute these derivatives; see Hoffmann and Chiang [22]. Thus, the formula for computing the first derivative in the x direction for the arbitrary field ϕ, where ϕ is a discrete field in 2-D, for example, $\phi = \phi_{(i,j)}$, is given by an implicit relation between the field values and its (x) derivative, at some neighboring points in the stencil:

$$\frac{1}{3}\frac{\partial \phi}{\partial x_{(i-1,j)}} + \frac{\partial \phi}{\partial x_{(i,j)}} + \frac{1}{3}\frac{\partial \phi}{\partial x_{(i+1,j)}} = \frac{1}{9}\frac{\phi_{(i+2,j)} - \phi_{(i-2,j)}}{4\mathrm{d}x} + \frac{14}{9}\frac{\phi_{(i+1,j)} - \phi_{(i-1,j)}}{2\mathrm{d}x} \quad (7)$$

where $(i, j) = [1 \cdots N_i, 1 \cdots N_j]$. Thus, a tridiagonal linear system has to be solved for each $j = \text{const}$ line ($j = 1 \cdots N_j$) of the mesh, to compute $\partial\phi/\partial x_{(i,j)}$, where $i = 1 \cdots N_i$. A similar procedure has been applied for computing the y derivatives, $\partial\phi/\partial y_{(i,j)}$. A direct tridiagonal linear system solver has been used, as described in Hoffmann and Chiang [22].

The compact finite-difference formula presented above has been applied for computing both x and y derivatives of the primitive variable vector, q. Once the $(\partial q/\partial x)^{\text{num}}_{(i,j)}$ and $(\partial q/\partial y)^{\text{num}}_{(i,j)}$ terms have been computed, the RHS of Eq. (6) can be assembled:

$$\mathbf{RHS}_{(i,j)} = -\mathcal{A}_{(q_0)}\left(\frac{\partial q}{\partial x}\right)^{\text{num}}_{(i,j)} - \mathcal{B}_{(q_0)}\left(\frac{\partial q}{\partial y}\right)^{\text{num}}_{(i,j)} + \mathbf{S}^{\text{num}}_{(i,j)} \quad (8)$$

Note that we made the hypothesis that q_0 is constant (uniform background flow conditions); the matrices $\mathcal{A}_{(q_0)}$ and $\mathcal{B}_{(q_0)}$ are constant throughout the domain and have to be computed just once, leading to very efficient numerics for sound propagation when using LEE.

IV. Temporal Discretization

High order temporal discretization has to be used in conjunction with the high order spatial discretization, to reduce the number of time steps, thus the computational effort for the simulation. A fourth-order explicit Runge–Kutta scheme has been used in the present work.

Replacing (8) in the semidiscrete Eq. (6), one obtains

$$\frac{\partial q}{\partial t_{(i,j)}} = \mathbf{RHS}_{(i,j)} \quad (9)$$

The fourth-order low-storage Runge–Kutta time advancement algorithm employed here is

$$q^0 = q^n \quad (10)$$

$$q^k = q^n + \alpha_k \cdot \mathrm{d}t \cdot \mathbf{RHS}(q^{k-1}) \qquad k = 1 \cdots 4 \quad (11)$$

$$q^{n+1} = q^4 \quad (12)$$

where α_k are the fourth-order Runge–Kutta stage coefficients defined by

$$\alpha_k = \frac{1}{4 - k + 1} \quad (13)$$

V. Filtering

Because the compact-finite difference scheme presented above has very small dissipation, efficient removal of spurious waves, that is, waves which cannot be resolved on the computational grid, is necessary. An option which is often used is the artificial selective damping by Tam et al. [23]. This approach is quite expensive, because additional terms have to be calculated in the differential equations. A more convenient way is to use suitable digital filters; see Vasilyev et al. [24]. Because the numerical scheme has extremely small dissipation, to avoid unrestricted growth of high-frequency (short wavelengths smaller than the computational grid) spurious oscillations to affect the solution, we apply a sixth-order explicit digital filter, of the following form (in 1-D) (see Lummer et al. [25]):

$$\bar{\Psi}_i = a_0 \Psi_i + \sum_{\varsigma=1}^{3} a_\varsigma \frac{\Psi_{i+\varsigma} + \Psi_{i-\varsigma}}{2} \tag{14}$$

where the filter coefficients are $a_0 = 0.6875$, $a_1 = 0.46875$, $a_2 = -0.1875$, $a_3 = 0.03125$ and $\bar{\Psi}_i$ is the filtered value of the quantity Ψ_i. We apply the same filter in both i and j directions at the same time, thus yielding the following formula in 2-D:

$$\bar{\Psi}_{i,j} = a_0 \Psi_{i,j} + \sum_{\varsigma=1}^{3} \frac{a_\varsigma}{4} (\Psi_{i+\varsigma,j} + \Psi_{i-\varsigma,j} + \Psi_{i,j+\varsigma} + \Psi_{i,j-\varsigma}) \tag{15}$$

This digital filter has been applied in the entire computational space and preserves the sixth-order accuracy of the numerical scheme. To apply these filters at boundaries we used appropriate order extrapolations.

For a $x = \text{const}$ boundary, the x derivatives of the primitive variable vector q have been computed using a high order one-sided finite difference, see Caraeni [21], whereas the y derivatives have been calculated using the above compact-finite differences.

Note that throughout the paper, the vector $q = (\rho, u, v, p)^T$ denotes the perturbation vector, whereas $\mathbf{q} = (\boldsymbol{\rho}, \mathbf{u}, \mathbf{v}, \mathbf{p})^T$ represents the instantaneous field vector; see relation (2).

VI. Boundary Conditions

Well-posed boundary conditions based on characteristic theory have been proposed in Caraeni [21]. In accord with this theory, the number of physical conditions must be equal to the number of characteristics that enter the computational domain. Thus, at supersonic inlets all characteristics enter the domain, therefore all (characteristic) variables have to be imposed; for LEE we need to impose the values of q which is the perturbation of a primitive variable vector. At supersonic outflow boundaries all characteristics exit the domain, hence the perturbations vector can be simply extrapolated from inside the computational domain to the boundary. Thus, supersonic inflow/outflow boundary conditions pose no special problems in aeroacoustics. In the following we will concentrate only on subsonic boundary conditions.

Acoustic (sound) and aerodynamic (entropy, vorticity, total enthalpy) disturbances, produced, for example, by turbulent flows, behave quite differently. Thus, in a subsonic regime the sound waves propagate in all directions at a speed equal to the sum of the sound speed and the local flow velocity, whereas entropic and vortical disturbances traveling with the flow speed, for example, are only convected downstream by the flow.

For brevity, let us consider here only the case of inflow/outflow boundary conditions on a line at $x = \text{const}$. Following Colonius [5], we can write the boundary conditions in terms of the characteristic variable $\mathbf{c}$, defined in this case as

$$\mathbf{c} = \begin{bmatrix} c_1 \\ c_2 \\ c_3 \\ c_4 \end{bmatrix} = \begin{bmatrix} p - \rho c_0^2 \\ \rho_0 c_0 \cdot u \\ p + \rho_0 c_0 \cdot u \\ p - \rho_0 c_0 \cdot u \end{bmatrix} \tag{16}$$

where $c_0^2 = \gamma p_0 / \rho_0$ is the square speed of sound, for the background flowfield. The corresponding (1-D) characteristic entropy variable, $c_1 = p - \rho c_0^2$, and vorticity variable, $c_2 = \rho_0 c_0 . u$, are transported downstream by the flow. Thus, at an inflow boundary these variables have to be specified, whereas at an outflow boundary these variables can be extrapolated from inside the domain. The characteristic variables $c_3 = p + \rho_0 c_0 \cdot u$, $c_4 = p - \rho_0 c_0 \cdot u$ correspond to forward, respectively, backward propagating sound waves. Their treatment is essential for obtaining the nonreflective characteristics at the inflow/outflow boundaries.

Two different inflow boundary conditions have been tested:

NRBC-I1, see Colonius [5]:

$$\begin{bmatrix} c_1 \\ c_2 \\ c_3 \end{bmatrix} = 0 \tag{17}$$

$$c_4 = c_4^{\text{int}} \tag{18}$$

NRBC-I2

$$\begin{bmatrix} c_1 \\ \nabla \times (u, v) \\ c_3 \end{bmatrix} = 0 \tag{19}$$

$$c_4 = c_4^{\text{int}} \tag{20}$$

where superscript "int" denotes a value that has been extrapolated from inside the domain at the boundary. Note that the condition $c_2 = 0$ in NRBC-I1 has been replaced by $\nabla \times (u, v) = 0$ in NRBC-I2, which effectively enforces a (zero) vorticity field at the inflow. If the incoming flow is rotational, then the specific value of the vorticity has to be imposed. This improvement produced a simple (non-PDE) inflow BC with good nonreflective characteristics, similar to the BCI2 condition by Colonius et al. [5].

Outflow boundary conditions with good nonreflective properties are more difficult to obtain. Four different outflow boundary conditions have been investigated here as follows:

NRBC-O1, see Colonius [5]:

$$c_4 = 0 \tag{21}$$

$$\begin{bmatrix} c_1 \\ c_2 \\ c_3 \end{bmatrix} = \begin{bmatrix} c_1 \\ c_2 \\ c_3 \end{bmatrix}^{\text{int}} \tag{22}$$

NRBC-O2, see Colonius [5]:

$$\frac{\partial c_4}{\partial t} = -u_0 \frac{\partial c_2}{\partial y} - v_0 \frac{\partial c_4}{\partial y} \tag{23}$$

$$\begin{bmatrix} c_1 \\ c_2 \\ c_3 \end{bmatrix} = \begin{bmatrix} c_1 \\ c_2 \\ c_3 \end{bmatrix}^{\text{int}} \tag{24}$$

NRBC-O3

$$c_4 = 0 \tag{25}$$

$$\begin{bmatrix} c_1 \\ \nabla \times (u, v) \\ c_3 \end{bmatrix} = \begin{bmatrix} c_1 \\ \nabla \times (u, v) \\ c_3 \end{bmatrix}^{\text{int}} \tag{26}$$

Note that, as compared to NRBC-O1, we propose to extrapolate the vorticity from inside the domain to the boundary. With this improvement the outflow BC will allow vortical structures to pass through the outflow boundary without perturbations. But, for NRBC-O3 boundary condition (and similar for NRBC-O1 and NRBC-O2), when a vortex reaches the exit boundary, a spurious pressure disturbance is produced in outflow and propagates inside

the domain, see the numerical tests below). To cure this problem we propose a new PDE based boundary condition for outflow:

NRBC-O4

$$\frac{\partial p}{\partial t} = -[u_0 + c_0.\text{sign}(u_0)]\frac{\partial p}{\partial x} - v_0\frac{\partial p}{\partial y} \tag{27}$$

$$\begin{bmatrix} c_1 \\ \nabla \times (u, v) \\ c_3 \end{bmatrix} = \begin{bmatrix} c_1 \\ \nabla \times (u, v) \\ c_3 \end{bmatrix}^{\text{int}} \tag{28}$$

We propose a new Eq. (27) for the time evolution of the pressure perturbation at the boundary. This equation has been obtained by modifying the equation for pressure valid inside the domain (29):

$$\frac{\partial p}{\partial t} + u_0\frac{\partial p}{\partial x} + v_0\frac{\partial p}{\partial y} + \gamma p_0\frac{\partial u}{\partial x} + \gamma p_0\frac{\partial v}{\partial x} = 0 \tag{29}$$

where the cross-derivative terms in pressure still remain, whereas the derivatives in the velocity perturbations have been dropped (these were the terms producing spurious pressure perturbations at the outflow boundary when a vortex was exiting the domain) and the normal derivative in pressure has been modified so that the equation preserves the correct speed of the outgoing pressure wave (e.g., if $u_0 > 0$, the outgoing pressure wave will have in outflow a velocity of $u_0 + c_0$). The transport equation (27) is integrated in time with the same fourth-order Runge–Kutta scheme we use for the interior of the domain. Using Eq. (27) and extrapolating the vorticity $\nabla \times (u, v)$ from inside the domain (instead of extrapolating the c_2 characteristic variable), we obtained improved nonreflective properties for our outflow BC, as the numerical experiments presented here will show. In fact we found that while using NRBC-O4 there is no need to consider an additional technique (such as absorbing layer, sponge layer, etc.) to additionally dump spurious pressure disturbances produced when vortical structures exit the domain.

The extent to which the initial/boundary-value problem is well posed is discussed in Caraeni [21].

Note that all inflow and outflow boundary conditions investigated here proved to have good nonreflective properties for sound propagation in an *irrotational* flow.

VII. Numerical Tests

To investigate the suitability of the above boundary conditions for computational aeroacoustics we propose four test cases: the propagation of an initially Gaussian-shaped pressure pulse, the uniform transport of a vortex, the propagation of the sound produced by a rotating quadrupole, and sound generation by the Kirchhoff vortex. All tests are done considering a uniform, subsonic mean flow.

A. Sound Propagating in Uniform Flow

First we study the sound propagation in a uniform flow. The sound wave is produced by a Gaussian-shaped pressure pulse introduced at $t = 0$ at the center of the 2-D computational domain $\mathcal{D} = \{x, y\} = [\{0 \cdots 10\} \times \{0 \cdots 10\}]$. The uniform flow conditions correspond to a low free-stream Mach number, $M_\infty = (0.04, 0.04)$. The initial pressure perturbation is given by the relation:

$$p = \delta_p \exp\left(-\frac{(x - x_0)^2 + (y - y_0)^2}{r_0^2}\right) \tag{30}$$

where δ_p is the pressure perturbation amplitude (here we take $\delta_p = 10^{-5} p_0$), r_0 is the characteristic dimension of the pulse, $r_0 = 1$, and the point of coordinates $\{x_0, y_0\}$ is the centroid of the 2-D domain $\mathcal{D}$. There is no perturbation in any of the other field variables, for example, ρ, u, v. The resulting propagating sound wave was simulated using the numerical scheme presented above, until the wave has left the domain. We found that all boundary conditions presented here performed well in this test case. For brevity we present here only the results obtained using our new boundary conditions: NRBC-I2 and NRBC-O4. Figures 1–5 present the sound wave at five

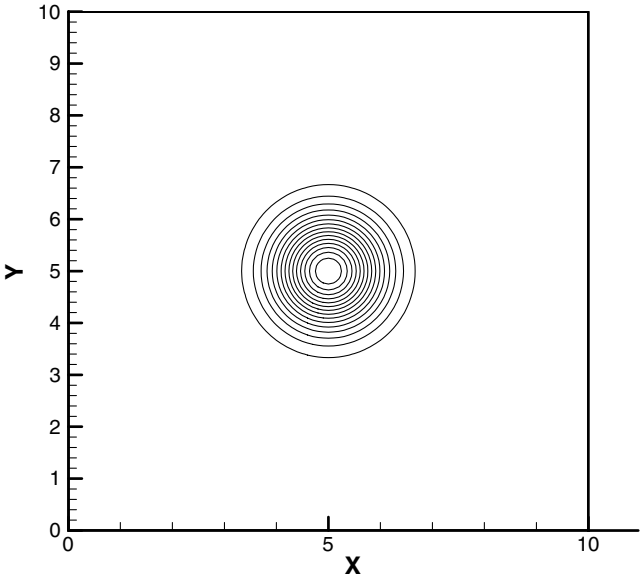

Fig. 1 Pressure perturbation at $t = 0$.

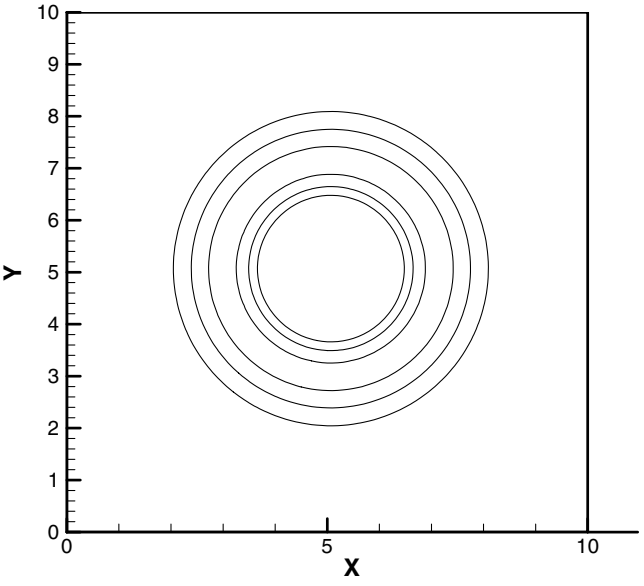

Fig. 2 Pressure perturbation at $t = \Delta t$.

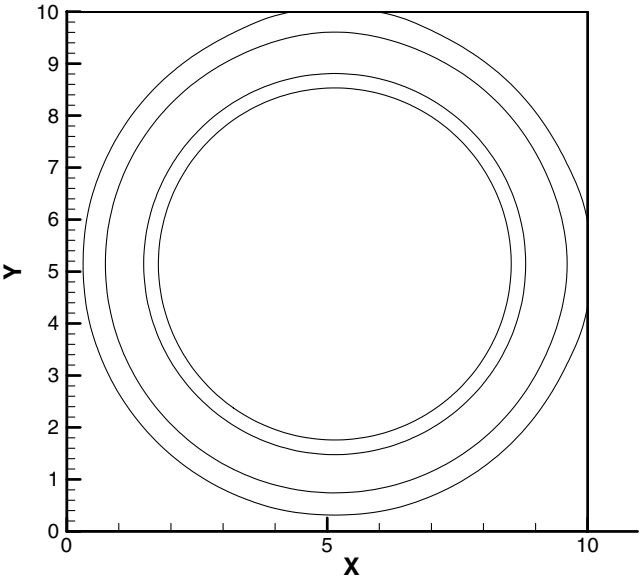

Fig. 3 Pressure perturbation at $t = 2\Delta t$.

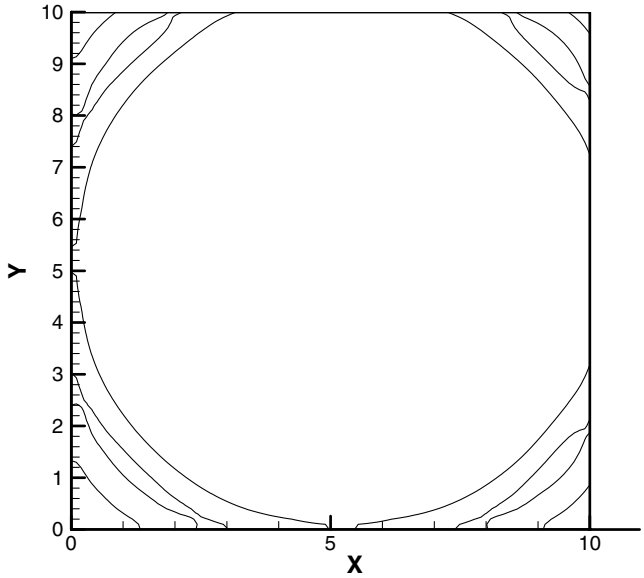

Fig. 4 Pressure perturbation at $t = 3\Delta t$.

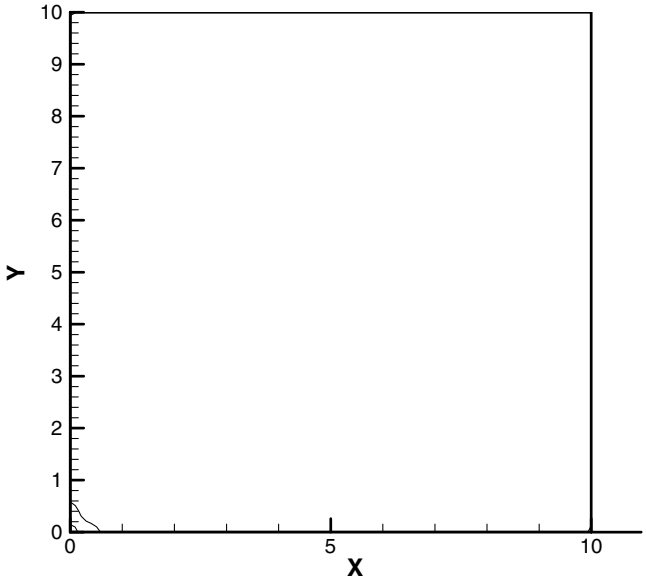

Fig. 5 Pressure perturbation at $t = 4\Delta t$.

successive moments in time, up to the point when the wave totally exited the domain. Notice that there are no spurious oscillations produced while the acoustic waves travel through boundaries.

The analytical solution for this initial value problem, as given in Bogey and Bailly [9]:

$$p(x,t) = \frac{\delta_p}{\beta}\int_0^\infty \xi^2 \exp\left[-\frac{\xi^2}{4\alpha}\right]\cos(t\xi)j_0(\xi\eta)\mathrm{d}\xi \tag{31}$$

where δ_p is the pressure perturbation amplitude (see above), $\alpha = \ell n\ 2$, $\beta = 2\alpha\sqrt{\pi\alpha}$,

$$\eta = [(x - M_x c_0 t)^2 + (y - M_y c_0 t)^2]^{1/2} \tag{32}$$

and the spherical Bessel function of the first kind and order zero j_0 is given by $j_0(z) = \sin(z)/z$.

Figure 6 displays the comparison between the numerical results, which have been obtained using the NRBC-I2 inflow boundary condition and the outflow boundary conditions NRBC-O1 to NRBC-O4, with the theoretical values for the pressure distribution on the outflow boundary at $x = 10$ m, for a given instant in time ($t = 3.5\Delta t$). Note that the results obtained with NRBC-O4 (solid line) are practically indistinguishable from the theoretical solution (symbols), but we can see that all outflow (and inflow) boundary conditions investigated here behave reasonably well for this test case.

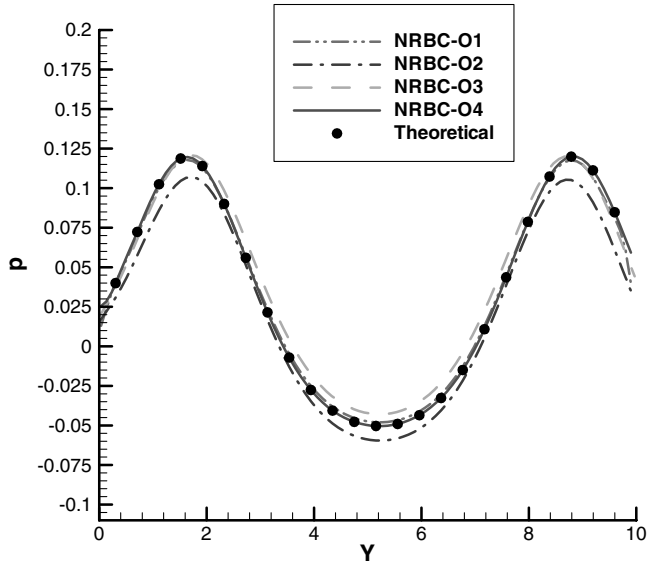

Fig. 6 Pressure perturbation on the outflow boundary ($x = 10$ m). Comparison between the numerical results and the theoretical values.

B. Vortex Propagating in Uniform Flow

Secondly, we investigate the transport of a vortex by uniform flow and the suitability of the different nonreflective boundary conditions for this kind of application. For brevity, we present here only the results that have been obtained using the NRBC-I2 inflow boundary condition, with different outflow boundary conditions. We consider the same 2-D computational domain $\mathcal{D} = \{x, y\} = [\{0 \cdots 10\} \times \{0 \cdots 10\}]$ and uniform flow conditions corresponding to a Mach number of $M_\infty = (0.5, 0.25)$. At time $t = 0$, the flowfield is perturbed such that a vortex is created, with a Gaussian-shaped vorticity distribution. The velocity perturbation (u, v) is given by

$$u = V_{\text{vortex}} \sin(\alpha)\bar{r}\exp(-\bar{r}^2/2) \tag{33}$$

$$v = V_{\text{vortex}} \cos(\alpha)\bar{r}\exp(-\bar{r}^2/2) \tag{34}$$

where $V_{\text{vortex}} = M_\infty c_0/100$, c_0 is the sound speed, $\tan(\alpha) = (y - y_0)/(x - x_0)$, and $\bar{r} = \sqrt{(x - x_0)^2 + (y - y_0)^2}/r_0$.

The pressure and density perturbations have been determined by considering that the perturbation introduced has to preserve locally the total enthalpy and entropy of the uniform flow. First, compute the local velocity, as a sum of mean-value plus perturbation:

$$\mathbf{u} = u_0 + u, \qquad \mathbf{v} = v_0 + v \tag{35}$$

then, determine the local pressure and density perturbations using the relations:

$$\mathbf{T} = \frac{p_0}{R_{\text{gas}}\rho_0} + \frac{(u_0^2 + v_0^2 - \mathbf{u}^2 - \mathbf{v}^2)}{2c_p} \tag{36}$$

$$p = p_0\left[\left(\mathbf{T}\frac{R_{\text{gas}}\rho_0}{p_0}\right)^{\frac{\gamma}{\gamma-1}} - 1\right] \tag{37}$$

$$\rho = \frac{p + p_0}{R_{\text{gas}}\mathbf{T}} - \rho_0 \tag{38}$$

The solution is advanced in time until the vortex completely leaves the domain, using the scheme described above. Figures 7–10 present the vorticity and pressure distributions at four successive moments in time, when using the NRBC-O1 outflow boundary condition.

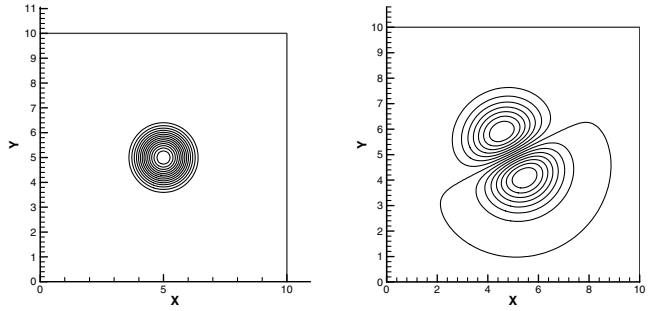

Fig. 7 Initial perturbed field. Vorticity and pressure field.

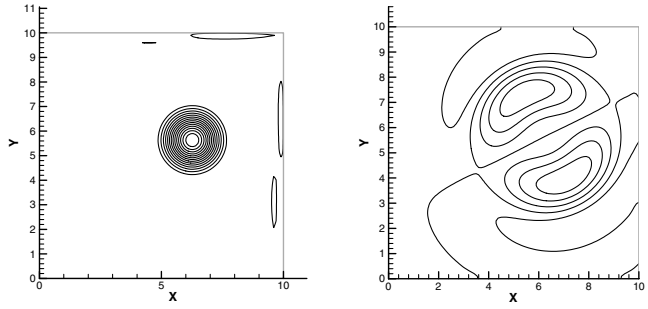

Fig. 8 Perturbed field. Vorticity and pressure field at $t = \Delta t$. Using NRBC-O1 boundary condition in outflow.

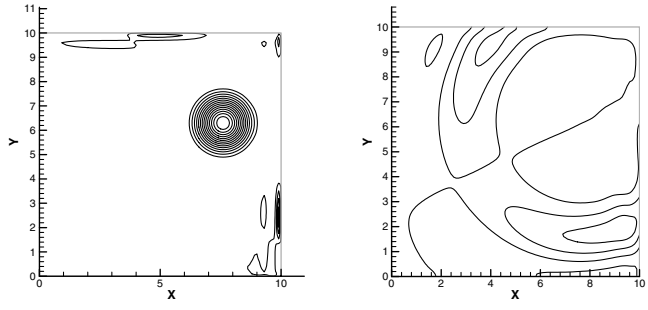

Fig. 9 Perturbed field. Vorticity and pressure field at $t = 2\Delta t$. Using NRBC-O1 boundary condition in outflow.

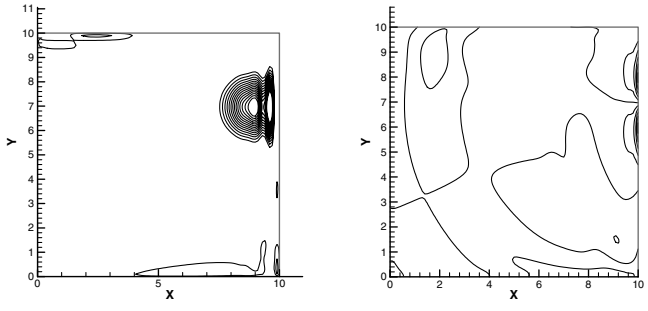

Fig. 10 Perturbed field. Vorticity and pressure field at $t = 3\Delta t$. Using NRBC-O1 boundary condition in outflow.

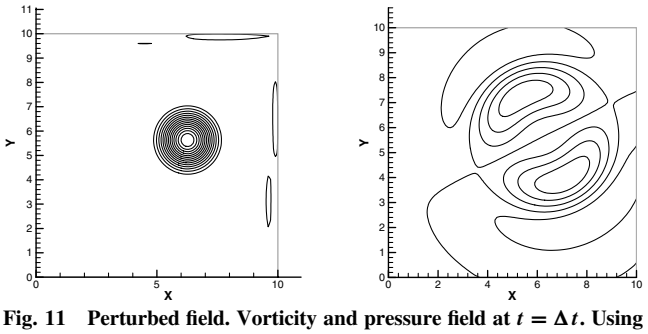

Fig. 11 Perturbed field. Vorticity and pressure field at $t = \Delta t$. Using NRBC-O2 boundary condition in outflow.

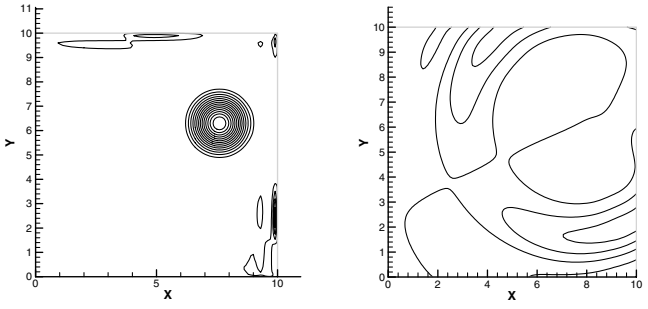

Fig. 12 Perturbed field. Vorticity and pressure field at $t = 2\Delta t$. Using NRBC-O2 boundary condition in outflow.

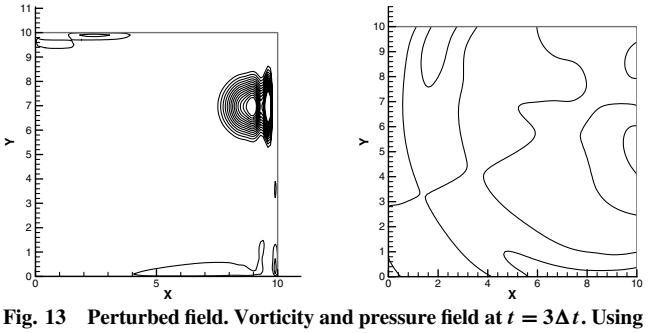

Fig. 13 Perturbed field. Vorticity and pressure field at $t = 3\Delta t$. Using NRBC-O2 boundary condition in outflow.

Figures 11–13 and Figs. 14–16 display the pressure and vorticity distributions for the case when using NRBC-O2 and NRBC-O3, respectively.

Note for NRBC-O2 that the use of a PDE for the fourth characteristic variable c_4 did improve the behavior of the scheme, by reducing the pressure reflections at the outflow boundary. At the same time the use of vorticity extrapolation instead of c_2 extrapolation, when using NRBC-O3, reduced significantly the scheme's effect on the vorticity distribution at boundary. The new outflow condition NRBC-O4 combines the two ingredients presented above to produce an improved scheme: uses a PDE for the pressure perturbation at the boundary and extrapolates the vorticity from inside the domain to the boundary. Figures 17–19 present the vorticity and pressure distribution when using the new outflow condition, NRBC-O4.

Please note that when using NRBC-O4 the spurious reflection of pressure in outflow, due to the vortex exiting the domain, has disappeared and the vortex also leaves the domain freely without being perturbed.

To quantify the numerical error introduced by the use of the four different boundary conditions investigated here, the same flow situation is simulated on a much larger domain, $\mathcal{D} = \{x, y\} = [\{-45 \cdots 55\} \times \{-45 \cdots 55\}]$ and the pressure, velocity (vorticity) distribution on the boundary of our original (much smaller) domain is monitored. Note that the same grid resolution and Courant number have been used. We use the solution on the large domain as the reference solution, to assess the quality of our results obtained when using the four different nonreflective boundary conditions. Pressure data have been collected on the outflow boundary of the small domain at $x = 10$. Note that the size of the large domain is sufficient so that there are no spurious reflections from its boundaries during the actual simulation. This setup allows the errors from the boundary conditions to be isolated from the other discretization errors and to be quantified.

The numerical error is defined here as the normalized difference between the pressure perturbation computed on the large domain on the outflow boundary of the small domain at $x = 10$ and the pressure perturbation on the boundary of the small domain. The normalization

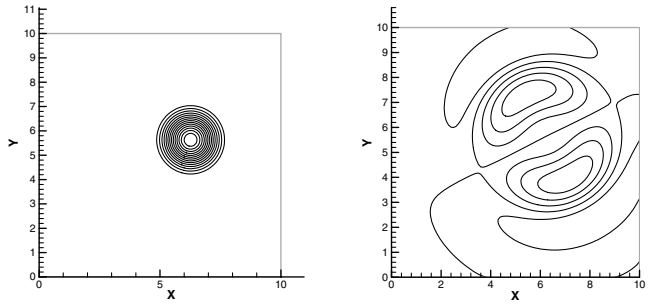

Fig. 14 Perturbed field. Vorticity and pressure field at $t = \Delta t$. Using NRBC-O3 boundary condition in outflow.

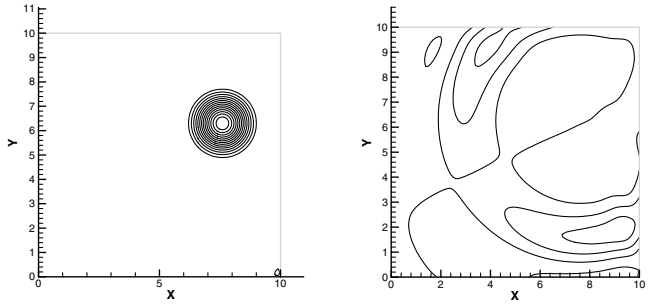

Fig. 15 Perturbed field. Vorticity and pressure field at $t = 2\Delta t$. Using NRBC-O3 boundary condition in outflow.

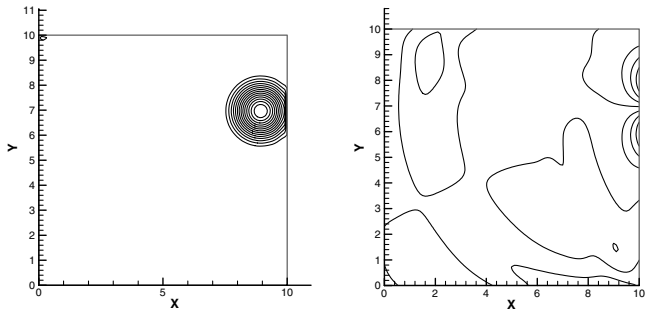

Fig. 16 Perturbed field. Vorticity and pressure field at $t = 3\Delta t$. Using NRBC-O3 boundary condition in outflow.

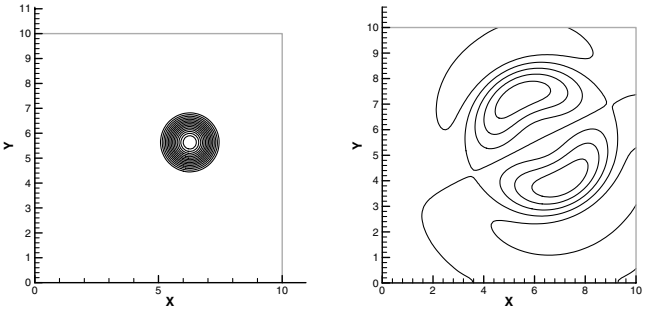

Fig. 17 Perturbed field. Vorticity and pressure field at $t = \Delta t$. Using NRBC-O4 boundary condition in outflow.

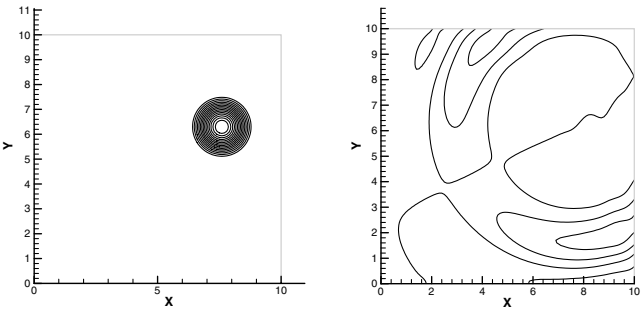

Fig. 18 Perturbed field. Vorticity and pressure field at $t = 2\Delta t$. Using NRBC-O4 boundary condition in outflow.

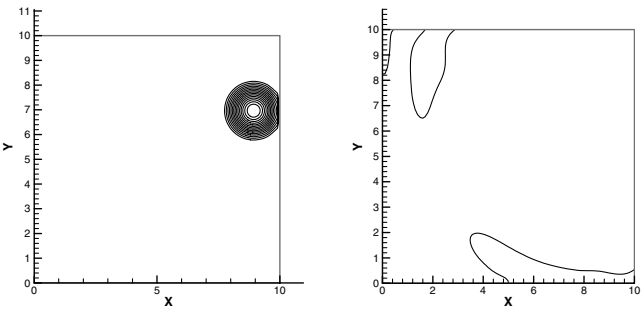

Fig. 19 Perturbed field. Vorticity and pressure field at $t = 3\Delta t$. Using NRBC-O4 boundary condition in outflow.

factor used here is $\rho(V_{\text{vortex}})^2/2$. Figure 20 shows the normalized error versus normalized time $\bar{t} = ta/L$, where a is the speed of sound, and L is half the size of the small domain. Our numerical results clearly show that NRBC-O4 gives the smallest error compared with the two boundary conditions by Colonius and Lele, that is, NRBC-O1 and NRBC-O2 or the modified boundary condition, NRBC-O3.

C. Propagation of Sound Produced by a Quadrupole

We study the propagation of the sound produced by a rotating quadrupole in uniform flow. The computational domain is $\mathcal{D} = \{x, y\} = [\{0 \cdots 10\} \times \{0 \cdots 10\}]$. The uniform flow conditions correspond to a low Mach number, $M_\infty = (0.01, 0.01)$. The pressure perturbations are introduced in the form of a source term for the pressure equation, given by the relation:

$$\mathbf{s}_p = \delta_p \bar{r} \exp\left(-\frac{\bar{r}^2}{2}\right) \sin(2\theta + \omega_R t) \cos(\omega_p t) \tag{39}$$

Here δ_p is the pressure source amplitude (here we take $\delta_p = 10^{-3} p_0$), $\bar{r} = \sqrt{(x - x_0)^2 + (y - y_0)^2}/r_0$ and r_0 is the characteristic dimension of the pulse, taken $r_0 = 1$, the point of coordinates $\{x_0, y_0\}$ is the centroid of the 2-D domain $\mathcal{D}$, $\tan\theta = y - y_0/x - x_0$, ω_R is the angular velocity of the rotating source, and ω_p is the angular velocity of the pulsation of the source, computed as a function of T. $T = |\mathcal{D}|/c_0$ is a characteristic time, $|\mathcal{D}|$ is the norm [1] of $\mathcal{D}$, and $c_0^2 = \gamma p_0/\rho_0$ is the sound speed. Thus, one can compute $\omega_R = \frac{\pi}{T}$ and $\omega_p = 8\omega_R$. There is no perturbation source introduced in any of the other field variables, for example, ρ, u, v. The sound waves produced were simulated using the above presented algorithm. The results presented here were obtained using the new inflow condition NRBC-I2 and the new outflow condition NRBC-O4.

Figures 21–25 display the sound waves at five successive moments in time. Notice that there are no spurious oscillations, as the acoustic waves travel through boundaries without being perturbed.

D. Sound Propagation by the Kirchhoff Vortex

Finally, we study the propagation of sound generated by a Kirchhoff vortex. The Kirchhoff vortex is a patch of constant vorticity ω inside an ellipse:

$$\frac{x^2}{a^2} + \frac{y^2}{b^2} = 1 \tag{40}$$

and zero vorticity outside, where a and b denote the semimajor and semiminor axes, respectively, of the ellipse. The Kirchhoff vortex rotates without change of shape with constant angular frequency Ω around the origin. The computational domain is $\mathcal{D} = \{x, y\} = [\{0 \cdots 10\} \times \{0 \cdots 10\}]$.

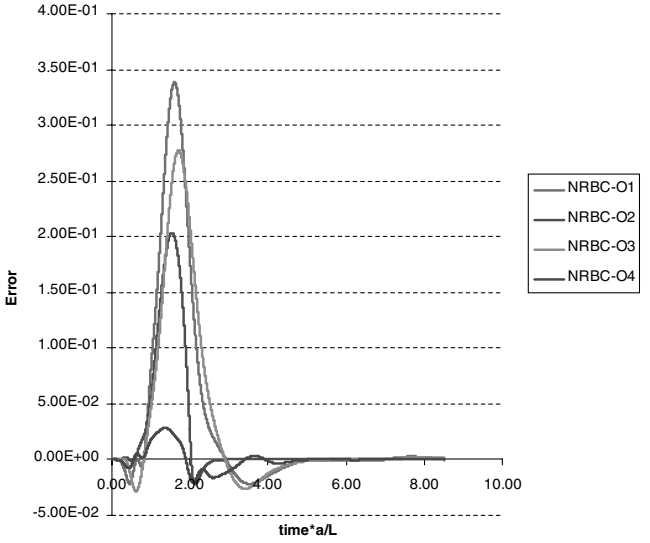

Fig. 20 Vortex propagating in uniform flow. Normalized error on outflow boundary as a function of time.

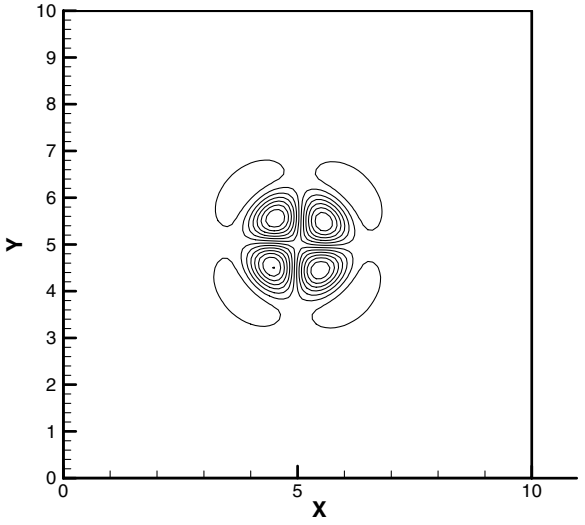

Fig. 21 Propagation of sound produced by a rotating quadrupole source. $t = 0$.

The perturbations are introduced in the form of source terms. Using the low Mach number approximation, the perturbations in the near field are given by the relations by Muller [26]:

$$\mathbf{s}_p(r,\theta,t) = -\frac{1}{2}\varepsilon\rho|u_{\text{ellipse}}|^2\left(\frac{\bar{a}}{r}\right)^2\cos[2(\theta-\Omega t)] \tag{41}$$

$$\mathbf{s}_u(r,\theta,t) = 2\bar{a}\varepsilon\Omega\sin[2(\theta-\Omega t)]\cos\theta \tag{42}$$

$$\mathbf{s}_v(r,\theta,t) = 2\bar{a}\varepsilon\Omega\sin[2(\theta-\Omega t)]\sin\theta \tag{43}$$

$$\mathbf{s}_\rho(r,\theta,t) = \frac{\mathbf{s}_p}{c_0^2} \tag{44}$$

where $|u_{\text{ellipse}}| = 2\bar{a}\Omega$ is the modulus of the velocity of the Kirchhoff vortex on the ellipse, $r = \sqrt{(x-x_0)^2+(y-y_0)^2}/r_0$ and r_0 is the characteristic dimension of the pulse, taken $r_0 = 1$, the point of coordinates $\{x_0, y_0\}$ is the centroid of the 2-D domain $\mathcal{D}$, and $\tan\theta = (y-y_0)/(x-x_0)$. ω_R is the angular velocity computed as function of T.

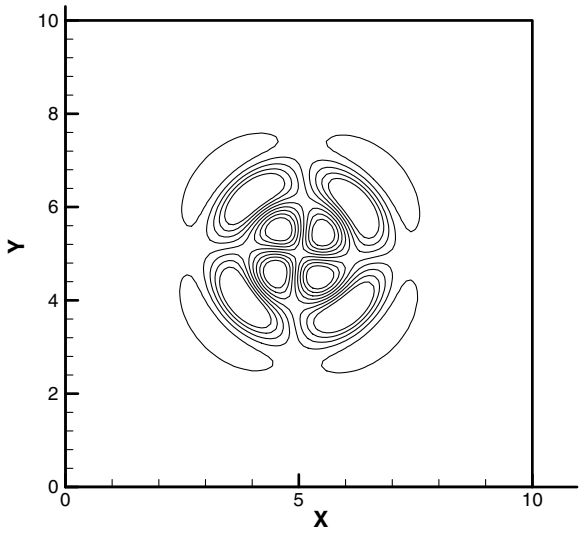

Fig. 22 Propagation of sound produced by a rotating quadrupole source. $t = \Delta t$.

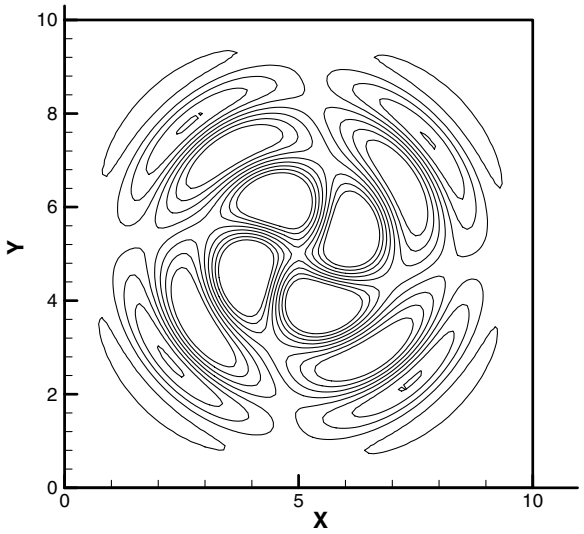

Fig. 23 Propagation of sound produced by a rotating quadrupole source. $t = 2\Delta t$.

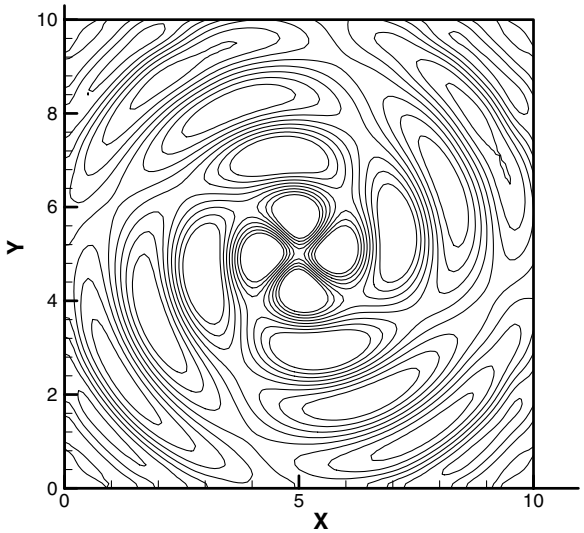

Fig. 24 Propagation of sound produced by a rotating quadrupole source. $t = 3\Delta t$.

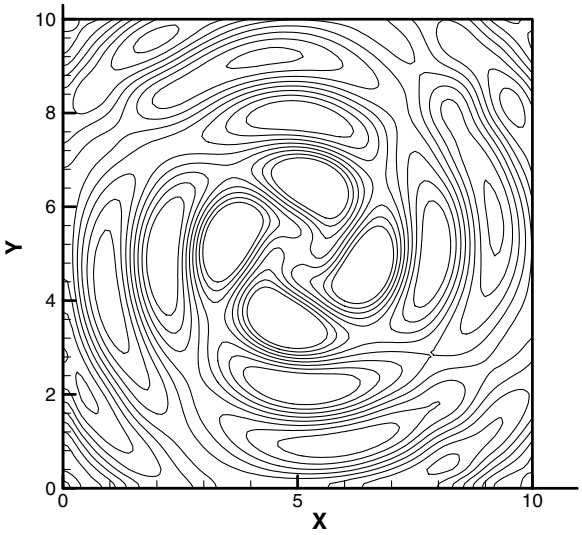

Fig. 25 Propagation of sound produced by a rotating quadrupole source. $t = 4\Delta t$.

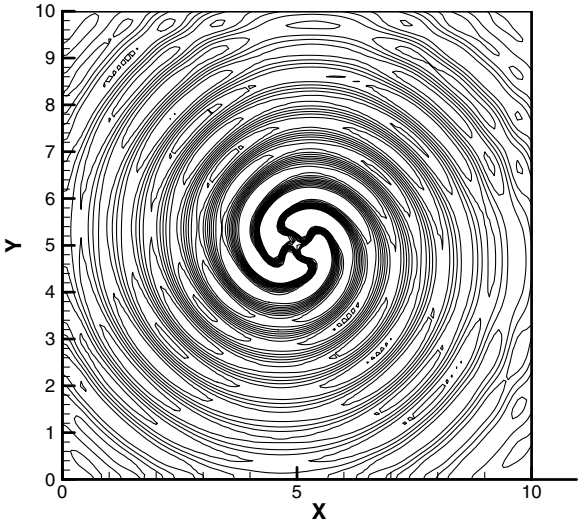

Fig. 26 Propagation of sound produced by Kirchoff vortex. $t = \Delta t$.

$T = \frac{|\mathcal{D}|}{c_0}$ is a characteristic time, and $|\mathcal{D}|$ is the norm of $\mathcal{D}$. One can compute $\omega_R = \frac{2\pi}{T}$, and then compute $\Omega = 5\omega_R$. The perturbations are introduced inside a circular region with $\bar{a} < r < 5\bar{a}$, where $\bar{a} = 0.1$ and $\varepsilon = 0.01$. $a = \bar{a}(1 + \varepsilon)$, and $b = \bar{a}(1 - \varepsilon)$.

The results presented here were obtained using the new inflow condition NRBC-I2 and the new outflow condition NRBC-O4. The sound waves spiral outwards from the rotating source and exit the domain smoothly. Figure 26 displays the sound waves at an instant in time.

VIII. Conclusions

A series of nonreflective boundary conditions have been investigated and a new outflow nonreflective boundary condition has been proposed with certain improved characteristics as compared with the other nonreflective boundary conditions investigated here. This nonreflective boundary condition is recommended for the direct computation of sound produced by turbulence.

References

[1] Givoli, D., "Nonreflecting Boundary Conditions," *Journal of Computational Physics*, Vol. 94, No. 1, 1991, pp. 1–29.

[2] Tsynkov, S. V., "Numerical Solution of Problems on Unbounded Domains: A Review," *Applied Numerical Mathematics*, Vol. 27, No. 4, 1998, pp. 465–532.

[3] Hagstrom, T., "Radiation Boundary Conditions for the Numerical Simulation of Waves, *Acta Numerica*, Vol. 8, Cambridge Univ. Press, Cambridge, MA, 1999, pp. 47–106.

[4] Giles, M. B., "Non-Reflecting Boundary Conditions for Euler Equations Calculations," *AIAA Journal*, Vol. 28, No. 12, 1990, pp. 2050–2058.

[5] Colonius, T., Lele, S. K., and Moin, P., "Boundary Conditions for Direct Computation of Aerodynamic Sound Generation," *AIAA Journal*, Vol. 31, No. 9, 1993, pp. 1574–1582.

[6] Tam, C. K. W., "Advances in Numerical Boundary Conditions for Computational Aeroacoustics," *Journal of Computational Acoustics*, Vol. 6, No. 6, 1998, pp. 377–402.

[7] Thompson, K. W., "Time Dependent Boundary Conditions for Hyperbolic Systems, I," *Journal of Computational Physics*, Vol. 68, Jan. 1987, pp. 1–24.

[8] Poinsot, T. J., and Lele, S. K., "Boundary Conditions for Direct Simulations of Compressible Viscous Reacting Flows," *Journal of Computational Physics*, Vol. 101, No. 1, 1992, pp. 104–129.

[9] Bogey, C., and Bailly, C., "Three-Dimensional Non-Reflective Boundary Conditions for Acoustic Simulations: Far-Field Formulations and Validation Test Cases," *Acta Acustica United with Acustica*, Vol. 88, No. 4, 2002, pp. 463–471.

[10] Watson, W. R., and Zorumski, W. E., "Periodic Time Domain Non-Local Non-Reflecting Boundary Conditions for Duct Acoustics," NASA TM-110230, Langley Research Center, March 1996.

[11] Bayliss, A., and Turkel, E., "Far-Field Boundary Conditions for Compressible Flows," *Journal of Computational Physics*, Vol. 48, Nov. 1982, pp. 182–199.

[12] Tam, C. K. W., and Webb, J. C., "Dispersion-Relation-Preserving Finite-Difference Schemes for Computational Acoustics," *Journal of Computational Physics*, Vol. 107, No. 2, 1993, pp. 262–281.

[13] Tam, C. K. W., and Dong, Z., "Radiation and Outflow Boundary Conditions for Direct Computation of Acoustic and Flow Disturbances in a Nonuniform Mean Flow," *Journal of Computational Acoustics*, Vol. 4, No. 2, 1996, pp. 175–201.

[14] Colonius, T., "Modeling Artificial Boundary Conditions for Compressible Flow," *Annual Review of Fluid Mechanics*, Vol. 36, 2004, pp. 315–345.

[15] Freund, J. B., "Proposed Inflow/Outflow Boundary Condition for Direct Computation of Aerodynamic Sound," *AIAA Journal*, Vol. 35, No. 4, April 1997, pp. 740–742.

[16] Berenger, J. P., "A Perfectly Matched Layer for the Absorption of Electromagnetic Waves," *Journal of Computational Physics*, Vol. 114, No. 2, 1994, pp. 185–200.

[17] Berenger, J. P., "Perfectly Matched Layer for the FDTD Solution of Wave-Structure Interaction Problems," *IEEE Transactions on Antennas and Propagation*, Vol. 44, No. 1, Jan. 1996, pp. 110–117.

[18] Hu, F. Q., "On Absorbing Boundary Conditions for Linearized Euler Equations by a Perfectly Matched Layer," *Journal of Computational Physics*, Vol. 129, No. 1, 1996, pp. 201–219.

[19] Tam, C. K. W., Auriault, L., and Canbuli, F., "Perfectly Matched Layer for Linearized Euler Equations in Open and Ducted Domain," AIAA Paper 98-0183, Jan. 1998.

[20] Hu, F. Q., "On Perfectly Matched Layers as an Absorbing Boundary Conditions," AIAA Paper 96-1664, May 1996.

[21] Caraeni, M.-L., "Developing Computational Tools for Modern Aeroacoustic Research," Ph.D. Thesis, Lund Institute of Technology, ISBN 91-628-5869-6, Sweden, 2003.

[22] Hoffmann, K. A., and Chiang, S. T.,"Computational Fluid Dynamics," 3rd ed., ISBN 0-9623731-2-5, Vol. 3, Engineering Education System, Wichita, KS, 2000, Chap. 22.

[23] Tam, C. K. W., Webb, J. C., and Dong, Z., "A Study of the Short Wave Components in Computational Acoustics." *Journal of Computational Acoustics*, Vol. 1, No. 1, 1993, pp. 1–30.

[24] Vasilyev, O., Lund, T., and Moin, P., "A General Class of Commutative Filters for LES on Complex Geometries," *Journal of Computational Physics*, Vol. 146, No. 1, 1998, pp. 82–104.

[25] Lummer, M., Delfs, J., and Lauke, T., "Simulation of the Influence of Trailing Edge Shape on Airfoil Sound Generation," AIAA Paper 2003-3109, 2003.

[26] Muller, B., "On Sound Generation by the Kirchhoff Vortex," Rept. 209/1998, Uppsala University, 1998.

K. Ghia
Associate Editor